University of **Reading**

More-persistent weak stratospheric polar vortex states linked to cold extremes

Article

Accepted Version

It is advisable to refer to the publisher's version if you intend to cite from the work. See Guidance on citing.

Published version at: http://dx.doi.org/10.1175/BAMS-D-16-0259.1

To link to this article DOI: http://dx.doi.org/10.1175/BAMS-D-16-0259.1

Publisher: American Meteorological Society

1   # More-persistent weak stratospheric polar vortex states linked to

2   # <u>cold</u> extremes

3   ## Authors

4   Marlene Kretschmer[*1,2], Dim Coumou[1,3], Laurie Agel[4,5], Mathew Barlow[4], Eli Tziperman[6],

5   Judah Cohen[*7]

6

7   ## Affiliations

8   [1]Potsdam Institute for Climate Impact Research, Earth System Analysis, Potsdam, Germany

9   [2]Department of Physics, University of Potsdam, Germany

10   [3]Institute for Environmental Studies (IVM), VU University Amsterdam

11   [4]Department of Environmental, Earth, and Atmospheric Sciences, University of

12   Massachusetts Lowell, Lowell, MA, USA

13   [5]Intercampus Marine Science Graduate Program, University of Massachusetts, MA, USA

14   [6]Department of Earth and Planetary Sciences and School of Engineering and Applied

15   Sciences, Harvard University, Cambridge, MA, USA

16   [7]Atmospheric and Environmental Research, Lexington, MA, USA

17

18   *Corresponding authors:

19   kretschmer@pik-potsdam.de (M.K.), jcohen@aer.com (J.C.)

20

Abstract

The extra-tropical stratosphere in boreal winter is characterized by a strong circumpolar westerly jet, confining the coldest temperatures at high latitudes. The jet, referred to as the stratospheric polar vortex, is predominantly zonal and centered around the pole; however, it does exhibit large variability in wind speed and location. Previous studies showed that a weak stratospheric polar vortex can lead to cold-air outbreaks in the mid-latitudes but the exact relationships and mechanisms are unclear. Particularly, it is unclear whether stratospheric variability has contributed to the observed anomalous cooling trends in mid-latitude Eurasia. Using hierarchical clustering, we show that over the last 37 years, the frequency of weak vortex states in mid to late winter (January and February) has increased which were accompanied by subsequent cold extremes in mid-latitude Eurasia. For this region 60% of the observed cooling in the era of Arctic amplification, i.e. since 1990, can be explained by the increased frequency of weak stratospheric polar vortex states, a number which increases to almost 80% when El Niño/Southern Oscillation (ENSO) variability is included as well.

Capsule

Over the last decades, the stratospheric polar vortex has shifted towards more frequent weak states which can explain Eurasian cooling trends in boreal winter in the era of Arctic amplification.

Introduction

Despite global warming, recent winters in the Northeastern United States (US), Europe and especially in Asia were anomalously cold. Some mid-latitude regions like Central Asia and eastern Siberia even show a downward temperature trend in winter over the past decades (Cohen et al. 2014a; McCusker et al. 2016). In contrast, the Arctic has been warming rapidly, challenging scientists to explain the so called warm Arctic – cold continents pattern in boreal winter (Shepherd 2016). Though there is general agreement that sea ice loss contributed to the warming of the Arctic via ice-albedo feedbacks (Screen and Simmonds 2010), it remains controversial whether observed mid-latitude cooling is related to internal atmospheric variability (Sun et al. 2016; McCusker et al. 2016), to tropical (Palmer 2014) or Arctic (Cohen et al. 2013; Cohen 2016) trends in teleconnection indices, or a combination of those.

Previous research showed that a weak stratospheric polar vortex (hereafter also referred to as 'polar vortex' or 'vortex') can affect surface weather via a downward influence of planetary waves (Baldwin and Dunkerton 2001; Hitchcock and Simpson 2014) which leads to cold air outbreaks in the mid-latitudes and a negative surface Arctic Oscillation signal (Cohen et al. 2013; Kolstad et al. 2010; Butler et al. 2014; Baldwin and Dunkerton 2001; Sigmond et al. 2013; Kretschmer et al. 2016). Moreover, it was shown that Sudden Stratospheric Warmings (SSW) can modulate the tropospheric flow for up to two months (Baldwin and Dunkerton 2001; Hitchcock and Simpson 2014) which can even offset the impact of El Niño Southern Oscillation (ENSO) events (Polvani et al. 2016). Consequently, including stratosphere activity in climate models significantly improves seasonal forecast skill for winter weather (Scaife et al. 2016; Sigmond et al. 2013). Despite this key role of the polar vortex for winter circulation and surface temperature, a quantitative analysis of the potential stratospheric role for the recent cooling trends has yet been lacking.

There are several metrics to describe polar vortex variability, extreme states and its coupling with the troposphere but the different indices do not necessarily capture all of these aspects. Often, the stratospheric impact on surface temperatures is analyzed in the context of Sudden Stratospheric Warmings (Polvani et al. 2016; Butler et al. 2014). Detection of SSWs is, however, sensitive to their exact definition, which varies throughout the literature (Butler et al. 2015). Moreover, SSWs are individual rare events and thus do not describe the overall behavior of the vortex. The tropospheric response of SSWs depends, however, on their temporal evolution and persistence in the stratosphere (Kodera et al. 2016; Runde et al. 2016). To study the recovery phase of extreme stratospheric events, Hitchcock et al. (2013) identified polar-night jet oscillation (PJO) events. These describe long-lasting anomalous warm temperatures in the stratospheric polar cap and are often preceded by SSWs, but approximately half of the SSWs recover rapidly from the abrupt warming (Hitchcock et al. 2013b).

Recently, machine learning approaches such as clustering algorithms have successfully been applied to study impacts of and changes in circulation patterns (Feldstein and Lee 2014; Horton et al. 2015; Lee and Feldstein 2013; Cheng and Wallace 1993), providing a promising data-driven tool to classify atmospheric fields. Motivated by these results, we perform cluster analysis on the daily extra-tropical stratosphere to identify its dominant spatial patterns and temporal evolution. This way we can study different vortex states as well as persistence of specific events. We analyze how long-term changes in polar vortex variability might have affected surface warming patterns.

Data

We use daily mean ERA-Interim (Dee et al. 2011) data from January 1979 to December 2015 leap days excluded. Data that were used to characterize the stratospheric polar vortex (geopotential height and zonal wind velocity at 10hPa) were provided on a 0.75° x 0.75° latitude-longitude grid. To study precursors and lagged effects of different polar vortex cluster events, we use gridded (3° x 3°) data of sea-level pressure, near surface temperature and poleward heat-flux ($v*T*$) at 100hPa, where v is the meridional wind velocity, T is the temperature and the asterisks denote the deviation from the zonal mean. We further use daily mean MERRA-2 (Molod et al. 2015) data from 1980-2015 to perform sensitivity analyses on the reanalysis product and clustering technique used.

Methods

We employ hierarchical clustering (Cheng and Wallace 1993) on the daily mean zonal wind velocity field poleward of 60°N at 10hPa. We chose this domain and level for consistency with most other SSW definitions and polar vortex studies (Butler et al. 2015). We limit the cluster analysis to the months January and February over the period 1979-2015, as these months show the strongest polar vortex variability. First we calculate the climatological anomalies for each day by subtracting their multi-year mean. Additionally, to account for the denser grid towards the pole, we apply area-weighting. There are $n = 2183$ daily observations (37 years times 59 days), each corresponding to a vector of length 19,680 (number of grid points in our domain) representing the state of the polar vortex on a particular winter day. The cluster algorithm groups days with similar extra-tropical

110 stratospheric wind fields in one cluster which can be represented by the composite of all

111 days assigned to it (see Appendix and Supplementary Information for more details).

112 We determine time series of the seasonal occurrence frequencies for each cluster which

113 ranges from zero (absent) to one (every day of the winter was assigned to that cluster).

114 Linear trends in occurrence frequency are calculated using a least-square fit regression

115 model and the slope was tested for significance using a two-sided Student´s t-test. We

116 define a cluster "event" as a period of consecutive days for which the same cluster is

117 identified.

118

More frequent weak polar vortex states

120 Our analysis reveals that seven is an appropriate choice for the number of clusters, providing

121 a sufficiently detailed overview of the spectrum of different polar vortex patterns, while still

122 allowing each pattern to describe a significant part of the total polar vortex phase space (see

123 Appendix and SI). This is also demonstrated by the relatively high mean pattern correlation

124 of 0.59, which is used to estimate how well the clusters represent the original data: the

125 area-weighted pattern correlation of each daily field to its cluster-composite is calculated,

126 and the average over all days represents a global measure of similarity.

127 Figure 1 shows the composite mean of the 10hPa geopotential height field for all seven

128 clusters, ordered by polar cap height (i.e. the area-weighted 10hPa geopotential heights

129 mean north of 60°N), starting with the strongest polar vortex cluster (thus with the lowest

130 polar cap height). Though clustering was performed on the zonal wind field, we present

131 geopotential heights for easier visualization of the different polar vortex shapes. The

132 associated zonal wind plots are given in Fig. S3. The patterns range from a strong

133 circumpolar vortex (cluster 1) to a slightly less-strong polar vortex (cluster 2), to

134 progressively weaker polar vortices with displaced vortex centers towards Eurasia (cluster 3,

135 5, 6) and North America (cluster 4) and finally a weak distorted vortex (cluster 7). Below the

136 cluster composites, time series of their seasonal frequency with a linear least square fit

137 trend line are displayed for each cluster. The strong vortex cluster (cluster 1) has a significant

138 (P = 0.047) downward linear trend of -0.2 $(37y)^{-1}$ whereas the weak vortex clusters 5, 6 and 7

139 increased in frequency, the last with a trend of 0.12 $(37y)^{-1}$ (P=0.146).

140 In principle, it is possible that trends in (seasonal) frequency are only the result of two or

141 more similar clusters with opposing trends that would cancel each other out if those clusters

142 were merged. To test this possibility, we calculate for each day the pattern correlation with

143 the composite mean of each cluster (Fig. S4, see SI for details). This thus quantifies how the

144 daily polar vortex patterns resemble the different clusters at each time-step. We find that

145 the strong vortex clusters (cluster 1, 2) exhibit a downward trend in pattern correlation

146 (P≈0.07). In contrast, the weak vortex clusters (cluster 6, 7) have upward trends (P≈0.07).

147 Thus, over the last 37 winters, the daily polar vortex state shifted towards the weaker cluster

148 patterns. This is consistent with the overall weakening of the stratospheric zonal wind field,

149 especially at the vortex edge over the continents (Fig. 2a, S5 for the polar cap mean). South

150 of 60°N the trends in zonal wind velocity are even upward, indicating an equatorward shift

151 and broadening in addition to the weakening of the vortex.

152 To test how well our cluster analysis reflects observed trends, we multiply the zonal wind

153 composite mean of each cluster with the slope of its frequency trend (Lee and Feldstein

154 2013). Summed for all clusters (Fig. 2b), this shows how much of the seasonal mean change

155 is explained by the change in frequencies and we find that it compares well with the actual

156 trend field (Fig. 2a). In fact, approximately 72% of the observed weakening north of 60°N is

157 already explained by the less frequent occurrence of the strong vortex cluster 1 and the

158 more frequent occurrence of the weak polar vortex cluster 7 (Fig. 2c).

159 To further test how the frequency of cluster events changes over time, we count the mean

160 seasonal occurrence in the first half (1979-1996) and the second half (1998-2015) of the

161 studied time-period for each cluster (Fig. 3a). We find that the frequency of cluster 7

162 increased significantly (using a bootstrapping approach; see Appendix) by 140% from on

163 average ca. 3 days per winter up to roughly 7 days (P<0.01). In contrast, the frequency of

164 cluster 1 halved from approximately 12 days per season to just 6 (P<0.05). The increased

165 frequency of cluster 7 days results from an increase in the persistence of cluster 7 events

166 (consecutive days assigned to cluster 7). Whereas in the first half of the studied time-period

167 the mean persistence of cluster 7 events was 5.3 days, it was significantly (P<0.01) longer in

168 the second half with events persisting on average 14.1 days (an increase by more than

169 160%). In contrast, the mean persistence of cluster 1 events was approximately 9 days in

170 both periods, but their occurrence dropped notably from 27 events in the first half to just 11

171 events in the latter half. Thus, the increase in cluster 7 days is due to longer events and the

172 decrease in cluster 1 days is due to less events.

173

Robust classification of weak polar vortex states

175 Our finding of more (less) frequent weak (strong) polar vortex days over the past winters is

176 robust and insensitive to the total number of clusters (from 2 to 20 clusters). Furthermore,

177 the cluster representatives and frequency trends of the strongest and the weakest cluster

178 are robustly identified and are mostly insensitive to the data-set (MERRA-2 instead of ERA-

179 Interim), clustering technique (using k-means or self-organizing maps instead of hierarchical

clustering), clustered variable (geopotential heights instead of zonal wind velocity) and pressure level (100hPa and the mean over 10-50hPa). Generally, clustering over lower pressure levels results in higher seasonal frequencies of weak polar vortex states. This is consistent with previous studies showing that disturbances of the upper stratospheric flow persist for longer when they descend to lower levels (Hitchcock et al. 2013b,a) and also with the fact that strong lower-stratospheric anomalies often coincide with tropospheric circulation anomalies (Baldwin and Dunkerton 2001) which, are not necessarily observed at higher levels. More precise information how the different tests compare can be found in the Supplementary Information (Fig. S6-S15).

Our clustering methodology is also consistent with other metrics to classify extremely weak states of the stratospheric polar vortex. All starting days of major SSWs in January and February, as detected by Charlton and Polvani (2007), are assigned to the weak vortex clusters 6 and 7 (Fig. S17), which also coincide with polar-night oscillation events (Fig. S16, Hitchcock et al. 2013b). In summary, the different sensitivity tests show that a cluster approach applied at 10hPa provides a robust and appropriate methodology to study the occurrence and persistence of weak polar vortex events as well as their coupling with lower stratospheric pressure levels.

Links to surface temperature

The tropospheric response to weak polar vortex states can influence surface weather for up to two months (Baldwin and Dunkerton 2001; Hitchcock and Simpson 2014; Sigmond et al. 2013). Further, the tropospheric response is more pronounced if the stratospheric recovery is slow following a vortex disturbance (Kodera et al. 2016; Runde et al. 2016). Thus, an

203 increase in more persistent weak polar vortex states, i.e. longer-lived cluster 7 events, could

204 potentially influence winter temperatures. In other words, the moderate changes in the

205 mean vortex state (Fig. S5) are much less relevant for surface conditions than the increased

206 persistence of extremely weak states.

207 To study the relationship of cluster 1 and 7 events with surface weather, we create

208 composites of (detrended) near-surface temperature (Fig. 4). As expected, strong vortex

209 states (cluster 1) coincide with mild temperatures in the Eastern US and Northern Eurasia

210 and cold temperatures over Alaska and Greenland (Fig. 4a). In contrast, during weak vortex

211 states (cluster 7), anomalously cold temperatures are observed in Northern Eurasia whereas

212 Canada is anomalously warm (Fig. 4b). Thus, the increased frequency in cluster 7 during

213 recent winters might be linked to the surface cooling trends over Eurasia. To test this, we

214 first determine different linear regression models onto mean winter (JF) near-surface

215 temperature at each grid-point and plot their R^2 values (Fig. 5), indicating how much of the

216 observed temperature variability is explained by the linear model. To account for potential

217 biases due to trends in the regressors and the temperature time-series, we detrended the

218 variables first. Though polar cap height (PCH) variability can explain already some seasonal

219 temperature variability (Fig. 5b), regression by cluster 7 seasonal frequency gives higher R^2

220 values, significant over extended regions, including Central Siberia, Eastern Canada and the

221 Western Atlantic sector but not the United States (Fig. 5c). The combination of ENSO

222 (described by the mean winter Nino3.4 index) and the seasonal frequency of cluster 7

223 further improves the results over the Pacific and parts of the United States (Fig. 5d) but

224 ENSO alone has very little influence on Eurasian temperature variability (Fig. 5a). Note that

225 the correlation between the detrended cluster 7 frequency time-series and the detrended

226 Nino3.4 index is only 0.01, showing that they are almost completely independent.

227 Next, we calculate the temperature trends at each grid-point for each of the regression

228 models (Fig. 6a-c). For consistency with previous studies analyzing the warm Arctic-cold

229 continent pattern (Sun et al. 2016; Cohen et al. 2013; Cohen 2016; McCusker et al. 2016), we

230 calculate trends over the era of Arctic amplification (Cohen et al. 2014a), i.e. from 1990

231 onward. We apply the regression parameters from the models calculated for the detrended

232 data from 1979-2015 (Fig. 5) to predict temperature trends using the non-detrended

233 regressors from 1990-2015. All models show a warm Arctic - cold continent pattern, with

234 much stronger cooling over Eurasia than over North America. The explanatory power of

235 ENSO (Fig. 6a) and polar cap heights at 10hPa (not shown) is small. In contrast, regression by

236 cluster 7 frequency (Fig. 6b) captures the observed Eurasian pattern well. The best

237 agreement with observations (Fig. 6d) is achieved with the models including both cluster 7

238 and the Nino3.4 index (Fig. 6c). Thus, although other factors certainly play a role as well, the

239 observed cooling trends over Eurasia (Fig. 6d) are well captured by the trend towards more-

240 persistent weak vortex states (Fig. 6b), something which can be further improved by

241 including tropical variability (Fig. 6c).

242

243 **Cold weather in Eurasia**

244 Several studies focused on Eurasia as the winter cooling trend has been more pronounced

245 (McCusker et al. 2016; Sun et al. 2016; Li et al. 2015; Mori et al. 2014). Indeed, our analyses

246 show that the relationship between weak polar vortex states and surface temperature is

247 much stronger for this region, as compared to the northeastern US (Fig. 4b, 5c, 6b).

248 Our predicted regression model based on cluster 7 correlates (r = 0.46, R^2 = 0.21)

249 significantly (P<0.01, according to a Student's t-test) with winter temperature averaged over

250 the Eurasian sector (15°-130°E, 50°-65°N, black box in Fig. 7a). This model performs much

251 better than a regression model based on the polar cap height (PCH) index at 10hPa (r = 0.26,

252 R^2 = 0.07, P = 0.11). Thus, the seasonal frequency of weak states is a better predictor for

253 Eurasian temperature variability than the polar cap mean. Moreover, the cluster 7 based

254 model explains ~60% of the domain-mean Eurasian cooling trend since 1990 (-0.95°K per

255 decade). For ENSO and the polar cap height this is respectively only 17% and 24%. When

256 ENSO is combined with cluster 7, the percent of the recovered cooling trend in Eurasia jumps

257 to 77%. This shows that the trend towards more-persistent weak polar vortex states can

258 explain most of the winter cooling trend over northern Eurasia.

259 Next we consider Eurasian cold extremes (defined as days when the temperature anomaly

260 over the Eurasian sector is below <-5°C, coinciding with the 10th percentile) and calculate the

261 relative occurrence frequency of each cluster. For the Null-Hypothesis, i.e. that stratospheric

262 variability plays no role, one would expect for each cluster a frequency during cold extremes

263 approximately equal to its occurrence over all winter days as displayed in Figure 1. Though

264 only 8.25% of all considered days were assigned to cluster 7 (Fig. 1), the likelihood of cluster

265 7 days roughly doubles to 17.2% if only cold days are considered (Fig. 7b), which is a

266 significant increase (P< 0.01, according to a chi-square test). The occurrence of cluster 6 days

267 also exceeds the expected frequency whereas the strong vortex clusters 1-3 occur less often

268 than statistically expected. Similarly, only 3% of the hottest days (exceeding the 90th

269 percentile) are cluster 7 days, which significantly (P<0.01) differs notably from the expected

270 occurrence of ~8% (not shown).

271 To assess the direction of causality between weak vortex states and Eurasian cold extremes

272 we perform lagged coincidence analysis. In the week before the onset of cluster 7 events,

273 most days are assigned to weak polar vortex states (51% cluster 6, 20% cluster 5), which

274 themselves are already associated with low temperatures anomalies over Eurasia. The mean

275 Eurasian temperature anomaly preceding cluster 7 events is -1.2°C but it reaches its

276 minimum value during cluster 7 events with an average anomaly of -1.9°C. Thus, cluster 7

277 days represent the peak of the polar vortex disturbance as well as the peak of the cold

278 anomalies over the northern Eurasian sector. Consistently, in the week before the onset of a

279 cold event, the likelihood of cluster 6 is anomalously high. If we merge cluster 6 and 7, the

280 mean Eurasian temperature during these weak vortex states is still negative (-1.1°C) but the

281 temperature in the preceding week is anomalously warm at +0.4°C. Thus, since weak vortex

282 events (clusters 6 and 7) are preceded by positive temperature anomalies in Eurasia, we

283 propose that the observed cooling trend in this region is more likely the consequence of the

284 vortex weakening rather than its cause. Moreover, we found that cluster 7 Granger causes

285 Eurasian temperature variability in winter and that the opposite is not true, which further

286 supports this assumption (see SI). This is also consistent with recent findings, showing that

287 cold spells over Eurasia are longer-lasting if accompanied by a weak polar vortex (Garfinkel

288 et al. 2017).

289

290 **Precursors and potential reasons for weak polar vortex states**

291 Finally, we analyze potential reasons for the observed trends in frequency of the polar

292 vortex cluster 1 and 7. Both observational and modeling studies have shown that strong

293 upward wave propagation in the upper troposphere can weaken the stratospheric flow

294 (Jaiser et al. 2013; Kretschmer et al. 2016; Kim et al. 2014; Polvani and Waugh 2004; Shaw et

295 al. 2014) as expected on theoretical grounds (Matsuno 1970) and is often preceded by

296 distinct sea level pressure anomalies (Baldwin and Dunkerton 1999; Cohen and Jones 2011;

297 Kretschmer et al. 2016). Therefore, we created composites of anomalies in sea level pressure

298 (30-10 days before the start date of cluster events) and meridional heat-flux v*T* at 100hPa

299 (10 days prior to the cluster events), which is a common proxy for vertical wave propagation

300 (Fig. 8a-d, showing only those for clusters 1 and 7). The choice of time-lags was motivated by

301 previous studies (Kretschmer et al. 2016; Kim et al. 2014; Cohen and Jones 2011) but the

302 results are also robust for time-shifts of a few days. In the month before the onset of a weak

303 polar vortex event, sea level pressure over most of northwest Eurasia is anomalously high

304 while sea level pressure over the Chukchi Sea, North America and the Northern Atlantic is

305 anomalously low (Fig. 8b). This pressure dipole is followed by an anomalously strong

306 poleward heat-flux over Northern Europe, Central Asia and Chukchi and Beaufort Seas and a

307 lower than normal heat-flux north over the Lena river and over northern Canada (Fig. 8d). In

308 contrast, strong polar vortex events are preceded by patterns of opposite sign of sea level

309 pressure and heat-flux anomalies but are of less amplitude (Fig. 8a, c).

310 Vice versa, to test if high western Siberian sea level pressure events are also followed by

311 weak polar vortex states (in a statistically significant way) we create an index of area-

312 averaged sea level pressure over the Ural Mountains region (45-70°N, 40-85°E) for

313 December and January (Cohen et al. 2014b; Kretschmer et al. 2016). We define strong

314 western Siberian High events when the index exceeds 1035hPa, which corresponds to the

315 93rd percentile. In the month following high sea level pressure over western Siberia in

316 December and January the frequency of cluster 7 events triples (from 8.25% to 26.1%,

317 P<0.01) whereas that of cluster 1 events halves (from 16.12% to 7.15%, P<0.01; see

318 Appendix). Thus, not only are cluster 7 events preceded by high sea level pressure over the

319 Ural Mountains but also high sea level pressure anomalies over western Siberia strongly

320 increase the likelihood of weak polar vortex states.

321 The cluster 7 v*T* precursor anomalies (Fig. 8d) correspond to a reinforcement of the

322 climatological poleward heat-flux, which has shown to lead to a weakened polar vortex

323 (Polvani and Waugh 2004; Dunn-Sigouin and Shaw 2015; Shaw et al. 2014). Moreover, the

324 sea level pressure composites for cluster 7 (Fig. 8b) are consistent with different studies

325 linking increased vertical wave propagation to tropospheric forcing (Kretschmer et al. 2016;

326 Feldstein and Lee 2014; Cohen and Jones 2011). Constructive interference with the

327 climatological high leads to more vertical wave activity in the upper troposphere and

328 thereby a weakening of the polar vortex (Feldstein and Lee 2014; Kretschmer et al. 2016;

329 Cohen et al. 2014b; Smith et al. 2010). Thus, the detected precursors of cluster 7 are in

330 accordance with known physical mechanisms of troposphere-stratosphere coupling.

331 The formation of anomalous high pressure over Northern Eurasia has been associated with

332 late autumn Barents and Kara sea ice loss and enhanced Eurasian October snow cover extent

333 (Kim et al. 2014; Kretschmer et al. 2016; Feldstein and Lee 2014; Cohen et al. 2014b).

334 Therefore, we speculate that these processes, which have been linked to Arctic amplification

335 (Cohen et al. 2014a; Overland et al. 2011) and which have also been reproduced by climate

336 models (Jaiser et al. 2016; Handorf et al. 2015), contributed to the patterns that favor a

337 weakened polar vortex represented by cluster 7 (Fig. 8b, d). Moreover, the involved time-lag

338 of approximately three months (Kretschmer et al. 2016) for these Arctic driven mechanisms

339 might explain why clustering with November and December data exhibits no trends in the

340 frequency of the different vortex clusters (Fig. S9). The negative sea level pressure anomalies

341 over the North Pacific for cluster 7 events (Fig. 8b) are also similar to patterns associated

342 with El Niño years, which are associated with a weak polar vortex (Baldwin and O'Sullivan

343 1995; Polvani et al. 2016). However, since different ENSO indices did not show any trend

344 over the last decades, the weakening polar vortex can probably not be explained by ENSO

345 related teleconnections. Nevertheless, the interplay between different tropical

346 teleconnections (Garfinkel and Hartmann 2008), natural variability (McCusker et al. 2016)

347 and variability in atmospheric responses to Arctic sea ice loss (Screen and Francis 2016) as

348 well as impacts of regional differences in sea ice decline (Sun et al. 2015) might influence the

349 stratospheric response. This interplay of possible causal drivers requires further analyses

350 using both climate models and observations (Overland et al. 2016).

351

Conclusion

353 Using cluster analysis, we identified dominant patterns of the stratospheric polar vortex in

354 boreal winter. We showed that the polar vortex weakening over the last four decades was a

355 result of more-persistent weak polar vortex states (cluster 7) and less frequent strong polar

356 vortex events (cluster 1) rather than an overall weakening. This shift in polar vortex states

357 can account for most of the recent winter cooling trends over Eurasian mid-latitudes via

358 stratosphere-troposphere coupling. The observed sea level pressure and heat-flux

359 precursors are in agreement with proposed physical mechanisms and can explain the

360 weakening of the polar vortex via a dynamical troposphere-stratosphere coupling.

361 Our analysis shows that the Eurasian cooling trend in the era of Arctic amplification can

362 largely be explained by polar vortex variability. Understanding the two-way link between

363 stratospheric and tropospheric circulation is hence essential for understanding winter

364 teleconnections in the northern hemisphere. Any improvements in winter-time seasonal

365 forecasts are likely to depend on our comprehension of competing drivers including the

366 influence of stratospheric variability (Sigmond et al. 2013; Kretschmer et al. 2016).

367

Acknowledgements

377

Appendix A: Methods

Clustering

The hierarchical cluster algorithm starts with n clusters (the starting vectors) and then iteratively merges two clusters until only one cluster (the mean over all vectors) exists. In each step the clusters with minimal distance are merged and their mean is calculated. Here we use Ward´s metric criteria, meaning that the two clusters to be merged at each step are those which result in the minimal increase in variance in the merged cluster, over all possible unions of clusters.

While more computationally demanding, hierarchical clustering has the advantage over other clustering techniques such as k-means or self-organizing maps (SOM), that no a-priori knowledge on the number of clusters is required. Each of the $n-1$ merging steps can be tracked back and the optimal number of clusters can thus be defined afterwards. The structure of the clustering process is visualized in a dendogram (Fig. S1) and is used to choose the number of clusters, although that choice does require some subjective judgment (see SI).

Statistical Analysis

For the comparison of the first and second half of the studies time-period (Fig. 3a) we test for significance by randomly picking blocks of 7 days of each season from the time-series which contains the cluster events. The length was chosen based on the mean event-length of all clusters during the whole period. The blocks are then shuffled between years and calendar slots creating artificial time-series, but the order within the blocks is maintained

400 (preserving the intra-seasonal auto-correlation of the original time-series). This way we

401 create a new time-series from which we calculate the frequency difference of the two data

402 halves. We do this 10,000 times and calculate the percentiles of the observed frequency

403 difference.

404

Composite plots

406 Before computing the temperature composites (Fig. 4), the data was detrended to prevent

407 biases due to trends in the occurrence of the clusters. The significance of the composites is

408 tested creating 10,000 artificial time-series by randomly picking and shuffling blocks of the

409 original time-series (with a block-length of five days). For each newly created time-series we

410 pick as many days as were used to form the composite but we also keep the start days and

411 length of the identified events from the original time-series to account for a potential

412 increase in auto-correlation during long-lasting cluster events. For the precursors we

413 similarly composite (Fig. 8) but we neglect polar vortex data of the very first 30 days (i.e.

414 01.01.1979-30.01.1979) since leading sea level pressure and v*T* values are not included in

415 the reanalysis datasets. The composites are then formed over the days preceding the onset

416 of the identified cluster event.

417

Coincidence analysis

419 To assess the coincidence of cold events in Eurasia and weak polar vortex states, we define

420 cold days as days when the mean temperature anomaly over the Eurasian sector is below a

421 certain threshold; e.g. below -5°C. Next we calculate the frequency of each cluster on cold

422 days and compare to the frequency of each cluster on all days. To test significance for the

423 observed frequency of a specific cluster *i*, we apply a chi-square test to the contingency table

424 containing the cluster number (occurrence of cluster *i*/ other than cluster *i*) and the extreme

425 event (occurrence of cold extreme/no cold extreme).

426 For the coincidence of anomalous sea level pressure over western Siberia and weak polar

427 vortex states, we calculate a baseline (i.e. climatological) frequency for each cluster based on

428 the 25-35 days following every day in December and January (neglecting December 1978

429 which is not included) which coincides with the absolute frequencies of the different clusters

430 as shown in Fig. 1. We compare that to the frequency for each cluster based on the 15 to 35

431 day periods following Siberian High events. To assess the significance, we create 1000

432 synthetic time series with the same number of Siberian High events as in observations, but

433 randomly distributed in time. This way we get a distribution of the cluster events frequencies

434 following Siberian High events and can calculate percentiles to get the corresponding P-

435 value.

References

Baldwin, M. P., and D. O'Sullivan, 1995: Stratospheric Effects of ENSO-Related Tropospheric Circulation Anomalies. *J. Clim.*, **8**, 649–667, doi:10.1175/1520-0442(1995)008<0649:SEOERT>2.0.CO;2.

——, and T. J. Dunkerton, 1999: Propagation of the Arctic Oscillation from the stratosphere to the troposphere. *J. Geophys. Res.*, **104**, 30937, doi:10.1029/1999JD900445.

Baldwin, M. P., and T. J. Dunkerton, 2001: Stratospheric harbingers of anomalous weather regimes. *Science*, **294**, 581–584, doi:10.1126/science.1063315.

Butler, A. H., L. M. Polvani, and C. Deser, 2014: Separating the stratospheric and tropospheric pathways of El Niño–Southern Oscillation teleconnections. *Environ. Res. Lett.*, **9**, 24014, doi:10.1088/1748-9326/9/2/024014.

Butler, A. H., and Coauthors, 2015: Defining Sudden Stratospheric Warmings. *Bull. Am. Meteorol. Soc.*, **96**, 1913–1928, doi:10.1175/BAMS-D-13-00173.1.

Charlton, A. J., and L. M. Polvani, 2007: A New Look at Stratospheric Sudden Warmings. Part I: Climatology and Modeling Benchmarks. *J. Clim.*, **20**, 449–469, doi:10.1175/JCLI3996.1.

Cheng, X., and J. M. Wallace, 1993: Cluster Analysis of the Northern Hemisphere Wintertime 500-hPa Height Field: Spatial Patterns. *J. Atmos. Sci.*, **50**, 2674–2696, doi:10.1175/1520-0469(1993)050<2674:CAOTNH>2.0.CO;2.

Cohen, J., 2016: An observational analysis: Tropical relative to Arctic influence on midlatitude weather in the era of Arctic amplification. *Geophys. Res. Lett.*, **43**, 5287–5294, doi:10.1002/2016GL069102.

——, and J. Jones, 2011: Tropospheric Precursors and Stratospheric Warmings. *J. Clim.*, **24**, 6562–6572, doi:10.1175/2011JCLI4160.1.

Cohen, J., J. Jones, J. C. Furtado, and E. Tziperman, 2013: Warm Arctic, Cold Continents. *Oceanography*, **26**, 1–12.

Cohen, J., and Coauthors, 2014a: Recent Arctic amplification and extreme mid-latitude weather. *Nat. Geosci.*, **7**, 627–637, doi:10.1038/ngeo2234.

——, J. C. Furtado, J. Jones, M. Barlow, D. Whittleston, and D. Entekhabi, 2014b: Linking Siberian snow cover to precursors of stratospheric variability. *J. Clim.*, **27**, 5422–5432.

Dee, D. P., and Coauthors, 2011: The ERA-Interim reanalysis: configuration and performance of the data assimilation system. *Q. J. R. Meteorol. Soc.*, **137**, 553–597, doi:10.1002/qj.828.

Dunn-Sigouin, E., and T. A. Shaw, 2015: Comparing and contrasting extreme stratospheric

469   events, including their coupling to the tropospheric circulation. *J. Geophys. Res. Atmos.*,
470   **120**, 1374–1390, doi:10.1002/2014JD022116.

471 Feldstein, S. B., and S. Lee, 2014: Intraseasonal and interdecadal jet shifts in the Northern
472   Hemisphere: The role of warm pool tropical convection and sea ice. *J. Clim.*, **27**, 6497–
473   6518, doi:10.1175/JCLI-D-14-00057.1.

474 Garfinkel, C. I., and D. L. Hartmann, 2008: Different ENSO teleconnections and their effects
475   on the stratospheric polar vortex. *J. Geophys. Res.*, **113**, D18114,
476   doi:10.1029/2008JD009920.

477 Garfinkel, C. I., S.-W. Son, K. Song, V. Aquila, and L. D. Oman, 2017: Stratospheric variability
478   contributed to and sustained the recent hiatus in Eurasian winter warming. *Geophys.*
479   *Res. Lett.*, **44**, 374–382, doi:10.1002/2016GL072035.

480 Handorf, D., R. Jaiser, K. Dethloff, A. Rinke, and J. Cohen, 2015: Impacts of Arctic sea-ice and
481   continental snow-cover changes on atmospheric winter teleconnections. *Geophys. Res.*
482   *Lett.*, **42**, n/a-n/a, doi:10.1002/2015GL063203.

483 Hitchcock, P., and I. R. Simpson, 2014: The Downward Influence of Stratospheric Sudden
484   Warmings*. *J. Atmos. Sci.*, **71**, 3856–3876, doi:10.1175/JAS-D-14-0012.1.

485 ——, and Coauthors, 2013a: Lower-Stratospheric Radiative Damping and Polar-Night Jet
486   Oscillation Events. *J. Atmos. Sci.*, **70**, 1391–1408, doi:10.1175/JAS-D-12-0193.1.

487 ——, T. G. Shepherd, and G. L. Manney, 2013b: Statistical Characterization of Arctic Polar-
488   Night Jet Oscillation Events. *J. Clim.*, **26**, 2096–2116, doi:10.1175/JCLI-D-12-00202.1.

489 Horton, D. E., N. C. Johnson, D. Singh, D. L. Swain, B. Rajaratnam, and N. S. Diffenbaugh,
490   2015: Contribution of changes in atmospheric circulation patterns to extreme
491   temperature trends. *Nature*, **522**, 465–469, doi:10.1038/nature14550.

492 Jaiser, R., K. Dethloff, and D. Handorf, 2013: Stratospheric response to Arctic sea ice retreat
493   and associated planetary wave propagation changes. *Tellus A*, **65**,
494   doi:10.3402/tellusa.v65i0.19375.

495 ——, T. Nakamura, D. Handorf, K. Dethloff, J. Ukita, and K. Yamazaki, 2016: Atmospheric
496   winter response to Arctic sea ice changes in reanalysis data and model simulations. *J.*
497   *Geophys. Res. Atmos.*, doi:10.1002/2015JD024679.

498 Kim, B.-M., S.-W. Son, S.-K. Min, J.-H. Jeong, S.-J. Kim, X. Zhang, T. Shim, and J.-H. Yoon, 2014:
499   Weakening of the stratospheric polar vortex by Arctic sea-ice loss. *Nat. Commun.*, **5**,
500   4646, doi:10.1038/ncomms5646.

501 Kodera, K., H. Mukougawa, P. Maury, M. Ueda, and C. Claud, 2016: Absorbing and reflecting
502   sudden stratospheric warming events and their relationship with tropospheric
503   circulation. *J. Geophys. Res. Atmos.*, **121**, 80–94, doi:10.1002/2015JD023359.

504 Kolstad, E. W., T. Breiteig, and A. A. Scaife, 2010: The association between stratospheric

505   weak polar vortex events and cold air outbreaks in the Northern Hemisphere. *Q. J. R.*
506   *Meteorol. Soc.*, **136**, 886–893, doi:10.1002/qj.620.

507 Kretschmer, M., D. Coumou, J. F. Donges, and J. Runge, 2016: Using Causal Effect Networks
508   to analyze different Arctic drivers of mid-latitude winter circulation. *J. Clim.*, 4069–4081,
509   doi:10.1175/JCLI-D-15-0654.1.

510 Lee, S., and S. B. Feldstein, 2013: Detecting ozone- and greenhouse gas-driven wind trends
511   with observational data. *Science*, **339**, 563–567, doi:10.1126/science.1225154.

512 Li, C., B. Stevens, and J. Marotzke, 2015: Eurasian winter cooling in the warming hiatus of
513   1998-2012. *Geophys. Res. Lett.*, **42**, 8131–8139, doi:10.1002/2015GL065327.

514 Matsuno, T., 1970: Vertical Propagation of Stationary Planetary Waves in the Winter
515   Northern Hemisphere. *J. Atmos. Sci.*, **27**, 871–883, doi:10.1175/1520-
516   0469(1970)027<0871:VPOSPW>2.0.CO;2.

517 McCusker, K. E., J. C. Fyfe, and M. Sigmond, 2016: Twenty-five winters of unexpected
518   Eurasian cooling unlikely due to Arctic sea-ice loss. *Nat. Geosci.*, **9**, 838–842,
519   doi:10.1038/ngeo2820.

520 Molod, A., L. Takacs, M. Suarez, and J. Bacmeister, 2015: Development of the GEOS-5
521   atmospheric general circulation model: evolution from MERRA to MERRA2. *Geosci.*
522   *Model Dev.*, **8**, 1339–1356, doi:10.5194/gmd-8-1339-2015.

523 Mori, M., M. Watanabe, H. Shiogama, J. Inoue, and M. Kimoto, 2014: Robust Arctic sea-ice
524   influence on the frequent Eurasian cold winters in past decades. *Nat. Geosci.*, **7**, 869–
525   873, doi:10.1038/ngeo2277.

526 Overland, J. E., K. R. Wood, and M. Wang, 2011: Warm Arctic—cold continents: climate
527   impacts of the newly open Arctic Sea. *Polar Res.*, **30**, doi:10.3402/polar.v30i0.15787.

528 ——, and Coauthors, 2016: Nonlinear response of mid-latitude weather to the changing
529   Arctic. *Nat. Clim. Chang.*, **6**, 992–999, doi:10.1038/nclimate3121.

530 Palmer, T., 2014: Record-breaking winters and global climate change. *Science (80-.).*, **344**,
531   803–804.

532 Polvani, L. M., and D. W. Waugh, 2004: Upward Wave Activity Flux as a Precursor to Extreme
533   Stratospheric Events and Subsequent Anomalous Surface Weather Regimes. *J. Clim.*, **17**,
534   3548–3554, doi:10.1175/1520-0442(2004)017<3548:UWAFAA>2.0.CO;2.

535 ——, and Coauthors, 2016: Distinguishing stratospheric sudden warmings from ENSO as key
536   drivers of wintertime climate variability over the North Atlantic and Eurasia. *J. Clim.*,
537   JCLI-D-16-0277.1, doi:10.1175/JCLI-D-16-0277.1.

538 Runde, T., M. Dameris, H. Garny, and D. E. Kinnison, 2016: Classification of stratospheric
539   extreme events according to their downward propagation to the troposphere. *Geophys.*
540   *Res. Lett.*, **43**, 6665–6672, doi:10.1002/2016GL069569.

Scaife, A. A., and Coauthors, 2016: Seasonal winter forecasts and the stratosphere. *Atmos. Sci. Lett.*, **17**, 51–56, doi:10.1002/asl.598.

Screen, J. A., and I. Simmonds, 2010: The central role of diminishing sea ice in recent Arctic temperature amplification. *Nature*, **464**, 1334–1337, doi:10.1038/nature09051.

——, and J. A. Francis, 2016: Contribution of sea-ice loss to Arctic amplification is regulated by Pacific Ocean decadal variability. *Nat. Clim. Chang.*, **6**, 856–860, doi:10.1038/nclimate3011.

Shaw, T. A., J. Perlwitz, and O. Weiner, 2014: Troposphere-stratosphere coupling: Links to North Atlantic weather and climate, including their representation in CMIP5 models. *J. Geophys. Res. Atmos.*, **119**, 5864–5880, doi:10.1002/2013JD021191.

Shepherd, T. G., 2016: Effects of a warming Arctic. *Science (80-.).*, **353**.

Sigmond, M., J. F. Scinocca, V. V. Kharin, and T. G. Shepherd, 2013: Enhanced seasonal forecast skill following stratospheric sudden warmings. *Nat. Geosci.*, **6**, 98–102, doi:10.1038/ngeo1698.

Smith, K. L., C. G. Fletcher, P. J. Kushner, K. L. Smith, C. G. Fletcher, and P. J. Kushner, 2010: The Role of Linear Interference in the Annular Mode Response to Extratropical Surface Forcing. *J. Clim.*, **23**, 6036–6050, doi:10.1175/2010JCLI3606.1.

Sun, L., C. Deser, and R. A. Tomas, 2015: Mechanisms of Stratospheric and Tropospheric Circulation Response to Projected Arctic Sea Ice Loss*. *J. Clim.*, **28**, 7824–7845, doi:10.1175/JCLI-D-15-0169.1.

——, J. Perlwitz, and M. Hoerling, 2016: What caused the recent "Warm Arctic, Cold Continents" trend pattern in winter temperatures? *Geophys. Res. Lett.*, **43**, 5345–5352, doi:10.1002/2016GL069024.

Figure Captions List

Figure 1:

Polar vortex clusters and their frequency trends. Composite mean of 10hPa geopotential heights values over all days that were assigned to the same cluster (clustering performed with zonal wind anomalies) and time series of normalized occurrence frequency in winter (JF) with least-square fit line. The number in parentheses denotes the total frequency occurrence (in percent) for the studied period.

Figure 2:

Trend in strongest and weakest polar vortex clusters explain the overall trend of the polar vortex. a) Seasonal-mean (JF) trend in zonal wind poleward of 40°N. Significant values (P<0.1) according to two-sided Student´s t-test are shown in hatches. b) Sum of all seven polar vortex cluster representatives multiplied by their trend in seasonal frequency. c) Same as b) but only for cluster 1 and 7.

Figure 3:

Average occurrence (in days) per winter of each cluster from 1979-1996 (light blue) and from 1998-2015 (dark blue) and the change in percent. Significant changes (P<0.05) are indicated in red.

586 **Figure 4:**

587 *Composites of detrended near-surface temperature during a) cluster 1 and b) cluster 7 days.*

588 *Significant values (P<0.05) are indicated with dots.*

589

590 **Figure 5:**

591 *Explained variance (R^2 values) of winter (JF) mean temperature for regression with a) winter*

592 *mean Nino3.4 index , b) winter mean polar cap height (PCH), c) cluster 7 frequency, d) cluster*

593 *7 frequency and the winter mean Nino3.4 index. Before calculation the regression models,*

594 *the linear trends of the regressors and the temperature was removed. Significant (P<0.05)*

595 *models according to F-test are indicated in hatches.*

596

597 **Figure 6:**

598 *a)-c) Linear trends in temperature as projected by the regression models in Figure 5a,c,d and*

599 *d) observed trends for the period 1990-2015.The regression models were calculated based on*

600 *detrended data from 1979-2015 and the projected trends are calculated for the undetrended*

601 *regressors from 1990-2015.*

602

603 **Figure 7:**

604 *Coincidence analysis for extreme cold days over a) the Eurasian sector (15°-130°E, 50°-65°N).*

605 *b) The deviation from the statistically expected occurrence frequency (as displayed in Figure*

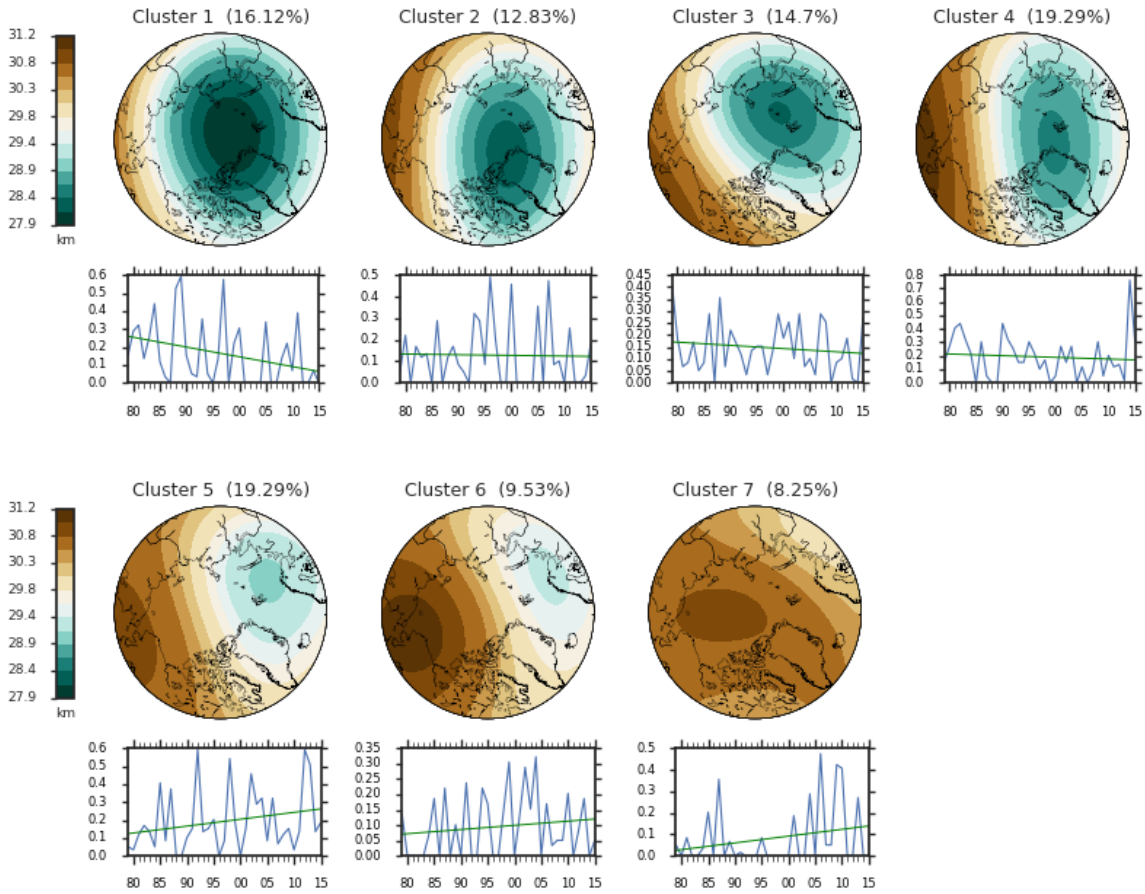606 *1) of each cluster is shown during cold days (<-5°C).*

607

608 **Figure 8:**

609 *Precursors to cluster events. Composite of (detrended) sea level pressure anomalies 30-10*

610 *days prior to start days of a) cluster 1 and b) cluster 7 events. c), d) as a), b) but for*

611 *(detrended) poleward heat-flux v*T* anomalies at 100hPa averaged 10 days before onset of*

612 *cluster event. In all panels, significant values (P<0.05) are indicated with dots.*

613

Figures

Figure 1:

Polar vortex clusters and their frequency trends. Composite mean of 10hPa geopotential heights values over all days that were assigned to the same cluster (clustering performed with zonal wind anomalies) and time series of normalized occurrence frequency in winter (JF) with least-square fit line. The number in parentheses denotes the total frequency occurrence (in percent) for the studied period.

Figure 2:

Trend in strongest and weakest polar vortex clusters explain the overall trend of the polar vortex. a) Seasonal-mean (JF) trend in zonal wind poleward of 40°N. Significant values (P<0.1) according to two-sided Student´s t-test are shown in hatches. b) Sum of all seven polar vortex cluster representatives multiplied by their trend in seasonal frequency. c) Same as b) but only for cluster 1 and 7.
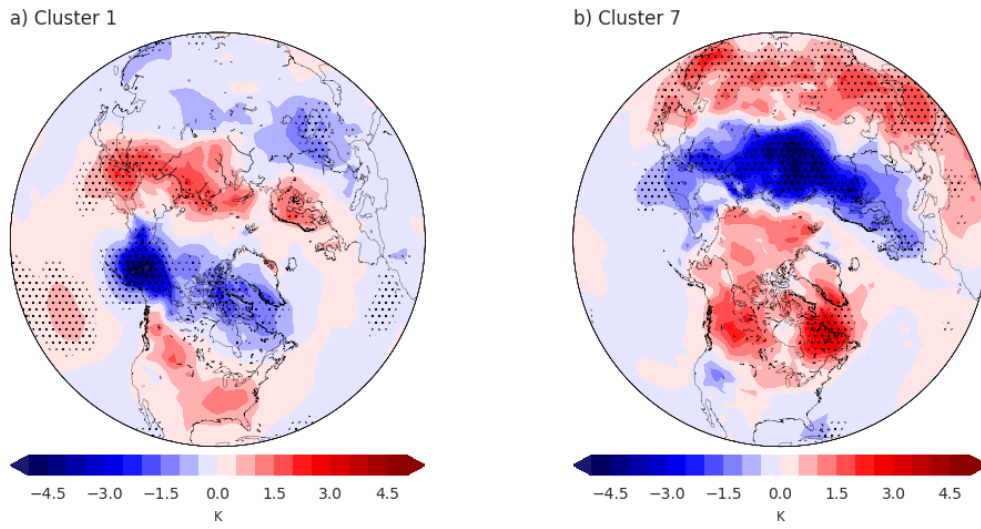
Figure 3:

Average occurrence (in days) per winter of each cluster from 1979-1996 (light blue) and from 1998-2015 (dark blue) and the change in percent. Significant changes (P<0.05) are indicated in red.
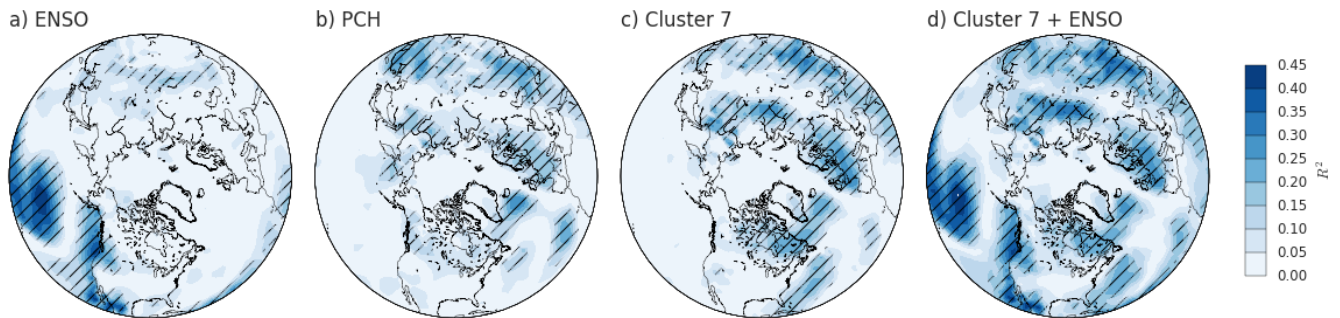
638 **Figure 4:**

639

a) Cluster 1   b) Cluster 7

640

641 *Composites of detrended near-surface temperature during a) cluster 1 and b) cluster 7 days.*

642 *Significant values (P<0.05) are indicated with dots.*

643

Figure 5:

646 Explained variance (R^2 values) of winter (JF) mean temperature for regression with a) winter

647 mean Nino3.4 index , b) winter mean polar cap height (PCH), c) cluster 7 frequency, d) cluster

648 7 frequency and the winter mean Nino3.4 index. Before calculation the regression models,

649 the linear trends of the regressors and the temperature was removed. Significant (P<0.05)

*650 models according to F-test are indicated in hatches.*

651

652 **Figure 6:**
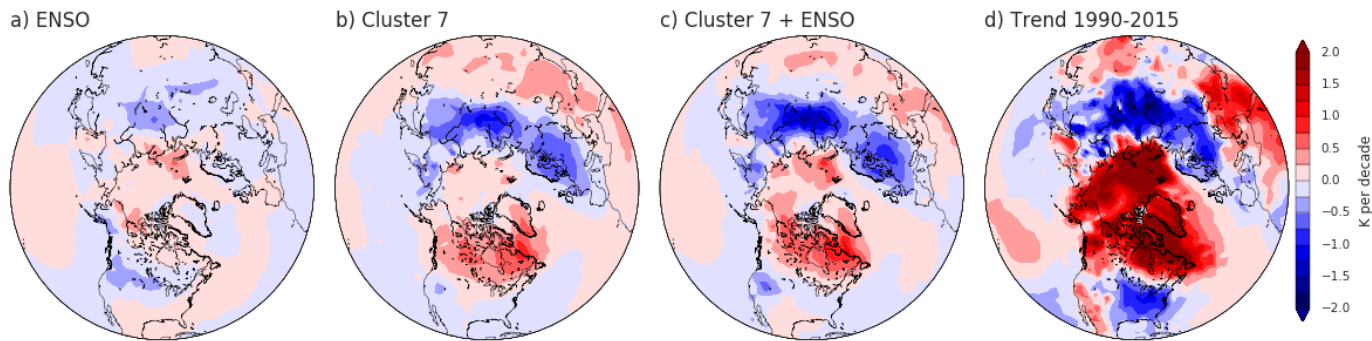
653

654 *a)-c) Linear trends in temperature as projected by the regression models in Figure 5a,c,d and*

655 *d) observed trends for the period 1990-2015.The regression models were calculated based on*

656 *detrended data from 1979-2015 and the projected trends are calculated for the undetrended*
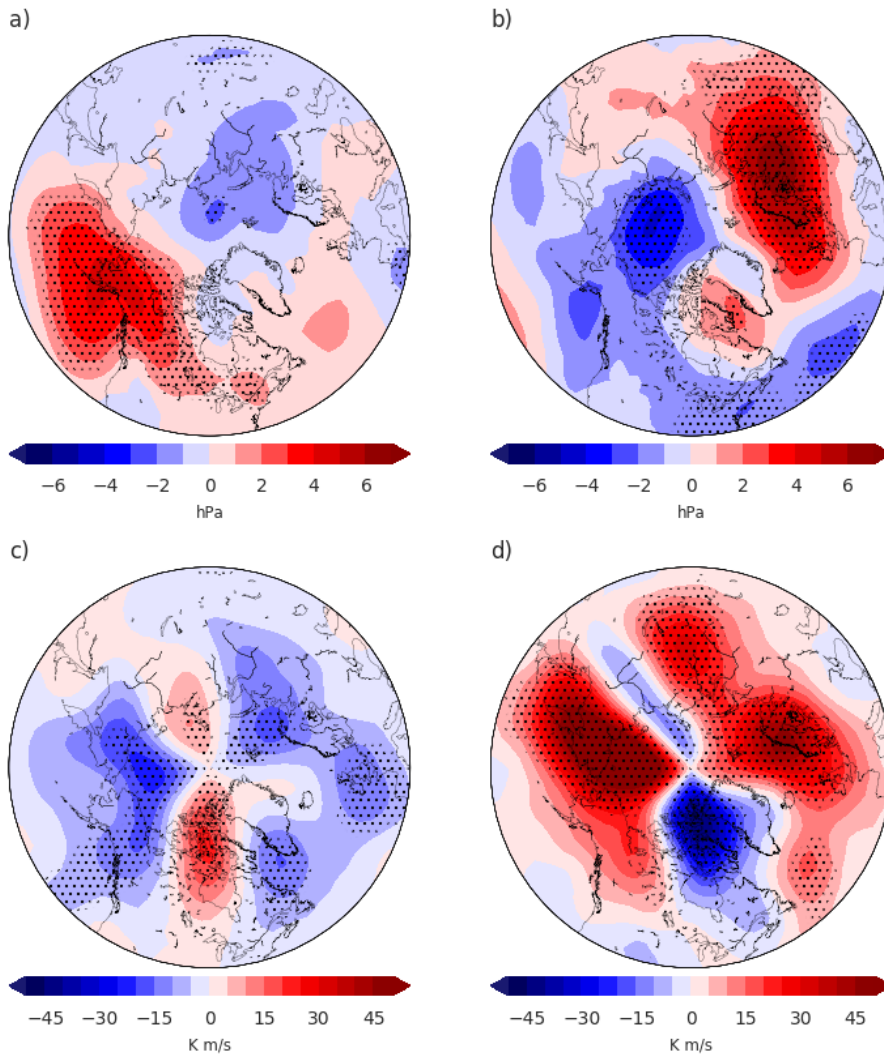
657 *regressors from 1990-2015.*
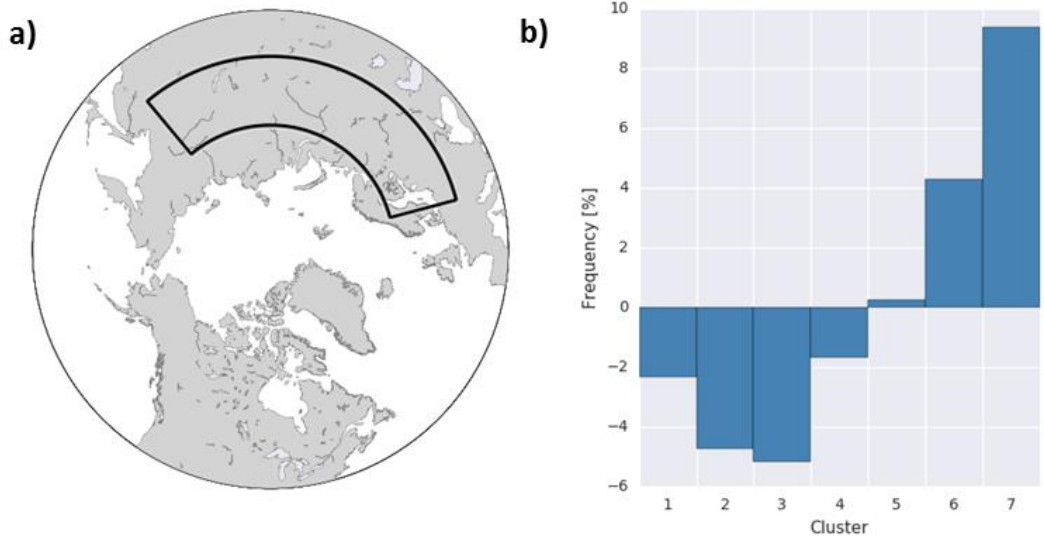
Figure 7:

Coincidence analysis for extreme cold days over a) the Eurasian sector (15°-130°E, 50°-65°N).

b) The deviation from the statistically expected frequency (as displayed in Figure 1) of each

cluster is shown during cold days (<-5°C).

Figure 8:

Precursors to cluster events. Composite of (detrended) sea level pressure anomalies 30-10 days prior to start days of a) cluster 1 and b) cluster 7 events. c), d) as a), b) but for (detrended) poleward heat-flux v*T* anomalies at 100hPa averaged 10 days before onset of cluster event. In all panels, significant values (P<0.05) are indicated with dots.